# Breathing Resistance and Ultrafine Particle Deposition in Nasal–Laryngeal Airways of a Newborn, an Infant, a Child, and an Adult

JINXIANG XI,[1,2] ARIEL BERLINSKI,[3,4] YUE ZHOU,[5] BRUCE GREENBERG,[3,6] and XIAWEI OU[3,6]

[1]Department of Systems Engineering, University of Arkansas at Little Rock, 2801 S. University Ave., EIT 536, Little Rock, AR 72204, USA; [2]Department of Mechanical and Biomedical Engineering, Central Michigan University, Mount Pleasant, MI, USA; [3]Arkansas Children's Hospital, Little Rock, AR, USA; [4]Department of Pediatrics, University of Arkansas for Medical Science, Little Rock, AR, USA; [5]Lovelace Respiratory Research Institute, Albuquerque, NM, USA; and [6]Department of Radiology, University of Arkansas for Medical Science, Little Rock, AR, USA

**Abstract**—As a human grows from birth to adulthood, both airway anatomy and breathing conditions vary, altering the deposition rate and pattern of inhaled aerosols. However, deposition studies have typically focused on adult subjects, results of which may not be readily extrapolated to children. This study numerically evaluated the age-related effects on the airflow and aerosol dynamics in image-based nose–throat models of a 10-day-old newborn, a 7-month-old infant, a 5-year-old child, and a 53-year-old adult. Differences in airway physiology, breathing resistance, and aerosol filtering efficiency among the four models were quantified and compared. A high-fidelity fluid-particle transport model was employed to simulate the multi-regime airflows and particle transport within the nasal–laryngeal airways. Ultra-fine particles were evaluated under breathing conditions ranging from sedentary to heavy activities. Results of this study indicate that the nasal–laryngeal airways at different ages, albeit differ significantly in morphology and dimension, do not significantly affect the total deposition fractions or maximum local deposition enhancement for ultrafine aerosols. Further, the deposition partitioning in the sub-regions of interest is different among the four models. Results of this study corroborate the use of the *in vivo*-based diffusion parameter ($D^{0.5}Q^{-0.28}$) over the replica-based parameter in correlating nasal–laryngeal depositions of ultrafine aerosols. Improved correlations have been developed for the four age groups by implementing this *in vivo*-based diffusion parameter as well as the Cunningham correction factor.

**Keywords**—Pediatric nasal physiology, Child–adult discrepancy, Infant nasal–laryngeal airways, Breathing in children, Health effects of ultrafine aerosols.

Address correspondence to Jinxiang Xi, Department of Systems Engineering, University of Arkansas at Little Rock, 2801 S. University Ave., EIT 536, Little Rock, AR 72204, USA. Electronic mail: jxxi@ualr.edu

## INTRODUCTION

Compared to adults, infants, and children are more susceptible to respiratory risks due to their immature defense mechanism and detoxification pathways.[21,27] Exposure to ambient toxicants in children may cause adverse effects such as nasal obstruction, sinusitis, and spread of infectious diseases.[50] Respiratory disease remains a leading cause of childhood morbidity in the U.S. and other developed countries and is a leading cause to childhood deaths worldwide.[6] Besides, children usually spend more time outdoors, breath faster, and therefore may receive a greater dose of PM per body weight than adults.

In contrast with potentially negative health effects, inhalation therapy for infants and children has been employed to deliver pharmaceutical aerosols to the lung via nasal route or to the nasal passages as the direct target. Aerosol delivery issues specific to children include lower tidal volumes, smaller airway size, and use of mask versus mouthpiece. With current devices, only a small amount of the applied dose reaches the target receptor in children.[20] Studies have shown that for adults about 10% of the administered drug reaches the lung whereas for infants and toddlers this percentage is usually less than 1%.[20] Therefore, children adapted methods, dose, and devices are likely to increase therapeutic options leading to improved inhalation therapy and medical outcomes.

A number of *in vivo* and *in vitro* studies have considered the deposition of nanoparticles in the nasal airway. *In vivo* studies that evaluated the nasal deposition of ultrafine aerosols or vapors in human subjects include Cheng *et al.*,[11,16] Swift and Strong,[69] Ginsberg *et al.*,[28] Bennett, *et al.*,[4,5] and Moller *et al.*,[49] among

others. The study of Cheng et al.[11] considered the deposition of aerosols ranging from 4 to 150 nm in 10 subjects and quantified variability in nasal geometries using MRI scans. Deposition was shown to be a function of nasal cavity surface area, minimum cross-sectional area, and shape complexity. *In vitro* studies provide the advantage of avoiding human subject testing and can determine depositions within specific regions of the nasal cavity. A number of *in vitro* studies have considered deposition of ultrafine aerosols in replicas of adult human noses.[10,14,15,30,32,38,41,68,78] The nasal geometries used in these studies are typically derived from medical scan data (CT and MRI) or casts of cadavers. Results of the available *in vitro* experiments are in general agreement with the deposition data from *in vivo* studies for ultrafine aerosols.[11] Regarding young subjects, Cheng et al.[13] measured deposition of ultrafine aerosols and thoron progeny in nose replicas of three children aged 1.5–4 years old. Based on a collection of children and adult nasal deposition data, Cheng et al.[13] suggested a best-fit correlation $\mathrm{DF} = 1 - \exp(-aD^{0.5}Q^{-0.125})$ for age groups ranging from 1.5 to 20 years old under quite breathing conditions. More recently, Golshahi et al.[29] measured depositions of inhaled ultrafine aerosols (13–100 nm) in CT-based replicas of nasal airways of ten infants aged 3–18 months. An empirical equation containing geometrical features of the nasal airways in the form of relevant non-dimensional parameters was proposed based on the infant deposition data. In both *in vivo* and *in vitro* tests, appreciable intersubject variability recurred in nasal filtrations,[3,25,39,62] likely due to differences in nasal anatomy and breathing patterns.

Previous computational fluid dynamics (CFD) studies have considered the transport and deposition of nanoparticles in the nasal cavity[26,35,40,42,46,48,63,64,71,74,75,79–81] Similar CFD studies have also evaluated the transport and absorption of dilute chemical species in the nasal passages.[17,61,82] Compared with *in vitro* and *in vivo* studies, CFD predictions have the advantage of providing detailed information on airflow and aerosol deposition, like hot spots that are more relevant to health outcome than the average deposition. However, to the authors' knowledge, very few CFD studies have been reported so far studying children nasal depositions, with one exception being Xi et al.[77] that examined the transport and depositions of micrometer particles. The general neglect of child or infant nasal airways in previous studies may largely be attributed to limited accessibility of pediatric medical images to CFD practitioners as well as the complexities involved in constructing physiologically realistic nasal passages. Concerning the age-related effect, several investigators have evaluated lung depositions of micrometer aerosols using scaled-down tracheobronchial models representa-tive of growing lungs at different ages.[2,18,54] In these studies, significant variations in micrometer particle lung deposition with respect to age were observed, with higher deposition in children than adults. However, no numerical study has been reported that evaluated the age-related effects on the breathing resistance and particle deposition in the nasal airways at different ages. Furthermore, few attempts seem to have been made to systematically quantify the detailed dimension and morphology of the developmental nasal anatomy to provide reference data for deposition prediction for different age groups.

The objective of this study is to assess the age effects on breathing resistance and nanoparticle deposition within the nasal–laryngeal airways in a systematic manner. There are four specific goals in this study: (1) developing anatomically accurate nose–throat models of a 10-day-old girl (newborn) and a 7-month-old girl (infant) based on CT images, (2) quantifying morphologic dimensions of the newborn and infant airway models and comparing to those of existing models of a 5-year-old boy and a 53-year-old adult; (3) characterizing the breathing resistance within the nasal passages during inhalation; and (4) evaluating the nasal deposition of ultrafine aerosols in the newborn, infant, child, and adult on a total, sub-regional, and localized basis. Results of this study may lead to a better understanding of the developmental respiratory physiology and the associated effects on children's health response to environmental pollutants, or the medical outcome from inhalation therapy for infants and children.

## METHODS

To achieve the above goals, anatomically realistic nose–throat models have been constructed based on CT/MRI images. Breathing scenarios ranging from sedentary through heavy activity conditions (i.e., 2–45 L/min) and inhaled particles ranging from 1 to 100 nm are considered (Table 1). Details of the geometry construction, inhalation conditions, pressure measurement, and fluid-particle transport models are described below.

TABLE 1. Test conditions for the airway models.

| Parameter | Range |
| --- | --- |
| $d_{\mathrm{p}}$ (nm) | 1–100 |
| Flow rate $Q_{\mathrm{in}}$ (L/min) | 2, 3, 5, 7, 10, 15, 20, 30, 45 |
| Cunningham factor $C_{\mathrm{c}}$ | 1.15–221 |
| Diffusivity $\tilde{D}$ (cm$^2$/s) | $5.44 \times 10^{-2}$–$2.84 \times 10^{-7}$ |
| Schmidt number $Sc = v/\tilde{D}$ | 2.92–$5.61 \times 10^{-5}$ |
| Particle Stokes number $St_k$ | $2.4 \times 10^{-8}$–$3.0 \times 10^{-3}$ |
| Inlet Reynolds number $Re$ | 189–5243 |

## Nasal–Laryngeal Airway Models

We use one example to illustrate the computer method to develop respiratory airway models based on medical images such as CT or MRI. Figures 1a–1d illustrate the procedures of translating 2-D images into a 3-D replica cast or computational model based on MRI scans of a healthy 5-year-old boy.[77] The multi-slice tracings (Fig. 1a) were first segmented using MIMICS (Materialise, Ann Arbor, MI) into 3-D model (Fig. 1b), which was further converted to a set of contours that define the airway of interest. Based on these contours, an internal surface geometry was constructed in Gambit 2.4 or ANSYS Workbench (Ansys, Inc.), which could be implemented either for dimension analysis, *in vitro* measurement or numerical modeling. To measure nasal breathing resistance, a life-size airway replica cast (Fig. 1c) was manufactured using a 3-D printer (Dimension 1200es, Eden Prairie, MN). For numerical analysis, an unstructured mesh was created using ANSYS ICEM (Ansys, Inc.) with fine near-wall elements (Fig. 1d). Respiratory geometry retained in this example extends from nostrils to throat including anatomic details such as epiglottal fold and laryngeal sinus (Fig. 1d). The resulting model is intended to faithfully represent the respiratory anatomy with only minor smoothing.

Similarly, existing CT scans of a 10-day-old girl (weight 3.46 kg and height 53 cm) and a 7-month-old girl (weight 9.3 kg and height 71 cm) were used to construct the nose–throat models and were compared with those of the 5-year-old child[77] and a 53-year-old male.[74,75] The CT scans of the two infants were provided by Arkansas Children Hospital with no health information disclosed, and their use has been approved by the UAMS Institutional Review Board. In order to quantitatively evaluate the flow field and aerosol depositions, the four airway models were each divided into five different sections (Fig. 2). In the main flow direction, subregions include the nasal vestibule and valve region (V&V), turbinate region (TR), nasopharynx (NP), pharynx and larynx.

## Inhalation and Wall Conditions

Steady inhalation was assumed for all simulations (nostrils) (Fig. 2). A wide spectrum of breathing conditions (2–45 L/min) was systematically studied and compared among the four subjects at different ages. In addition, inhalations representative of quiet breathing for the four subjects were also considered (Table 2). Based on published respiratory parameters,[22,24,60] the inhalation flow rate under quiet breathing were selected to be 3.8 L/min for the 10-day-old girl, 6.5 L/min for the 7-month-old girl, 11.2 L/min for the 5-year-old boy, and 18 L/min for the adult. Interestingly, the tidal volumes in the four subjects were observed to intimately correlate with the nasal–laryngeal airway volumes as shown in Table 3 (newborn–infant–child–adult ratio for tidal volume: 4.4%, 17.4%, 35.4%, 100% vs. airway volume: 6.4%, 18.8%, 40.3%, 100%). Based on the nostril areas in Table 4, the inlet velocities
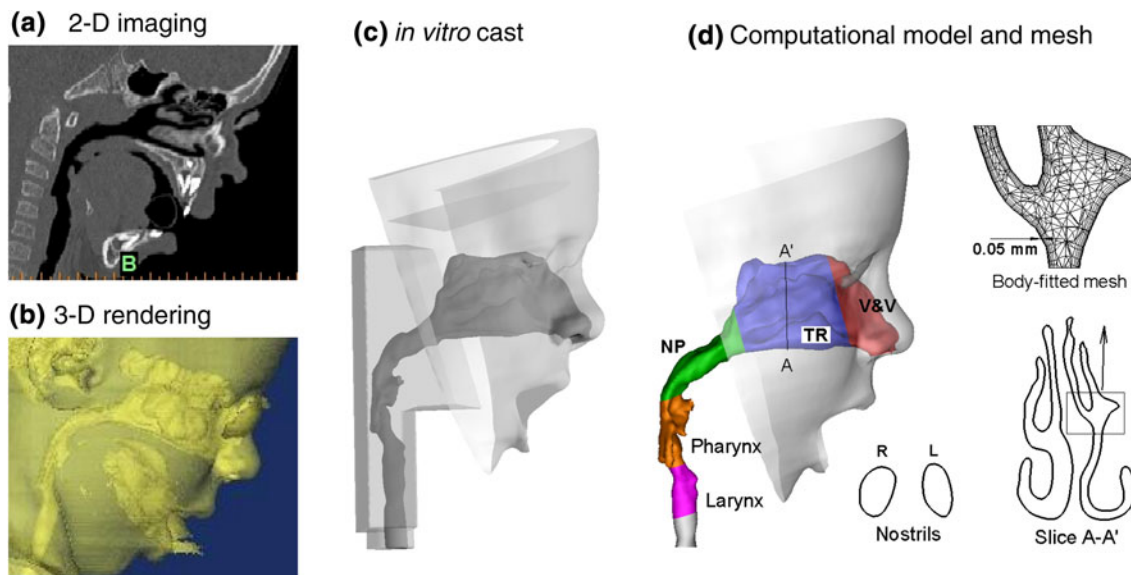


FIGURE 1. Procedures of 3-D rendering from medial images. (a) From the MRI scans of a 5-year-old boy, (b) a solid model of the airway was segmented using MIMICS, from which a surface model could be developed. This surface model can be either (c) fabricated into a hollow cast for *in vitro* experiments, or (d) meshed for numerical analysis. The nasal airway was divided into different anatomical sections: nasal vestibule and valve region (V&V), nasal turbinate (TR), nanopharynx (NP), pharynx, and larynx. The computational mesh is composed of approximately 1.75 million unstructured tetrahedral elements and fine near-wall grid.
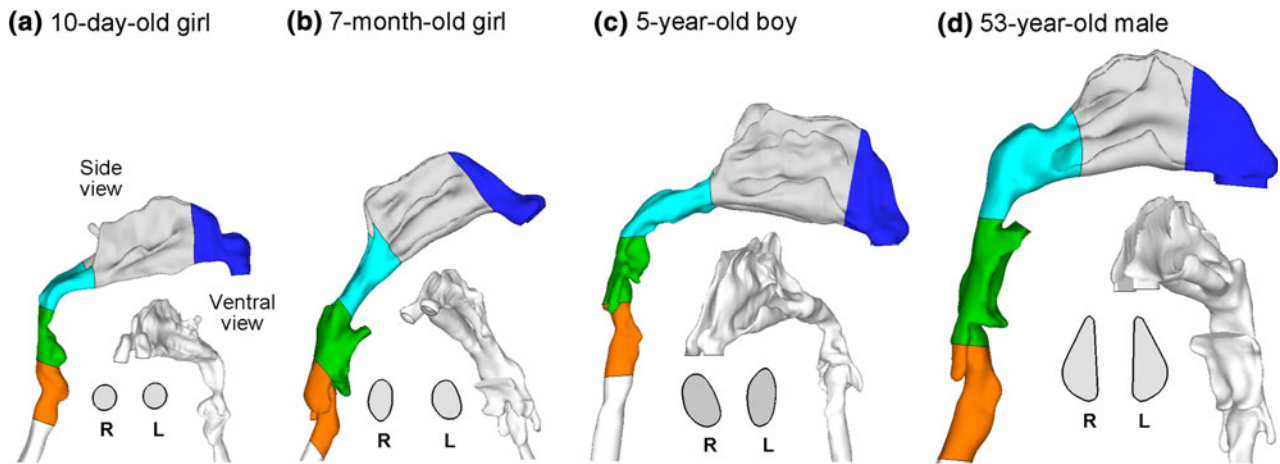
**FIGURE 2.** Image-based nasal airway model of (a) 10-day-old girl (neonate), (b) a 7-month-old girl (infant), (c) a 5-year-old boy (child), and (d) a 53-year-old male (adult).

**TABLE 2. Respiratory parameters under quiet breathing conditions at various ages.**

| Respiratory variable | 10 day | 7 month | 5 year | Adult |
|---|---|---|---|---|
| Frequency (min$^{-1}$) | 44 | 25 | 21 | 12 |
| I:E* ratio | 1:3 | 1:2 | 1:2 | 1:2 |
| Inhalation (s) | 0.34 | 0.8 | 0.95 | 1.67 |
| Tidal volume (mL) | 22 | 87 | 177 | 500 |
| TV ratio[‡] (%) | 4.4 | 17.4 | 35.4 | 100 |
| Flow rate (L/min) | 3.8 | 6.5 | 11.2 | 18.0 |
| Inlet velocity (m/s) | 1.91 | 1.84 | 1.84 | 1.48 |

*I:E ratio: inspiratory to expiratory ratio.
[‡]TV ratio: the ratio of tidal volume to that of the adult.

are similar among the four subjects under quite breathing conditions. Initial particle velocities were assumed to be the same as the local fluid velocity. The airway surface was assumed to be smooth and rigid with no-slip ($u_{wall} = 0$) and perfect absorption conditions.

### Pressure Measurement

Pressure difference between the inlet and outlet of the *in vitro* cast of the 5-year-old child was measured using a pressure meter (Magnehelic Gage, Dwyer Instrument Inc., Michigan City, IN). The inlets (i.e., nostrils) of the *in vitro* cast were open to room air, and a vacuum was connected to the outlet of the airway cast. The pressure meter was positioned about right after the outlet of the cast to measure the outlet pressure of the nose–throat model. Pressure drop was obtained for constant inhalation flow rates between 5 and 48 L/min by adjusting the valve in the vacuum line. The flow rate was measured at the outlet using a flow meter (Model 4140, TSI Inc., Shoreview, MN) positioned upstream of the flow valve.

### Numerical Methods

Flows in this study are assumed to be isothermal and incompressible. The mean inlet Reynolds number at the trachea varies from 189 to 5234. The maximum Reynolds number based on the hydraulic diameter of the glottal aperture is approximately 10,000. The low Reynolds number (LRN) $k$–$\omega$ model was selected to resolve the possible multi-regime flow dynamics that can coexist in the nasal airway due to its unique physiology.[77]

The transport and deposition of the nanoparticles are simulated with a well-tested discrete Lagrangian tracking model enhanced with near-wall treatment. The aerosols evaluated in this study had a density of 1.0 g/cm$^3$ and particle Stokes number ($St_k = \rho_p d_p^2 U / 18\mu D_h$) range of 0.00001–1.0. The inhaled particles were assumed to be dilute and had no influence upon the continuous-phase, i.e., one-way coupled particle motion. In our previous studies, the Lagrangian tracking model enhanced with user-defined routines was shown to provide close agreement with experimental deposition data in upper respiratory airways for both submicrometer[76] and micrometer particles.[73] To account for non-continuum effects of ultrafine particles, the Cunningham slip correction factor $C_c$ was computed using the expression of Allen and Raabe.[1]

$$C_c = 1 + \frac{\lambda}{d_p}\left(2.34 + 1.05 \exp\left(-0.39\frac{d_p}{\lambda}\right)\right) \quad (1)$$

where $\lambda$ is the mean free path of air, assumed to be 65 nm. The influence of non-uniform flow fluctuations in the near-wall region was taken into account by implementing an anisotropic turbulence model proposed by Matida *et al.*[47] The particle trajectories within the first-layer computational mesh above the

**TABLE 3. Nasal airway dimension of the four airway models of different ages.**

| Anatomy* | Volume, $V$ (cm$^3$) | | | | Surface area, $A$ (cm$^2$) | | | | Effective diam., $d_e$‡ (cm) | | | |
|---|---|---|---|---|---|---|---|---|---|---|---|---|
| | 10 day | 7 month | 5 year | Adult | 10 day | 7 month | 5 year | Adult | 10 day | 7 month | 5 year | Adult |
| V&V | 0.79 | 1.25 | 3.37 | 5.50 | 7.45 | 9.75 | 23.74 | 35.58 | 0.43 | 0.52 | 0.57 | 0.62 |
| TR | 1.57 | 2.83 | 11.03 | 12.63 | 21.09 | 35.63 | 107.34 | 112.59 | 0.30 | 0.32 | 0.41 | 0.45 |
| NP | 0.48 | 1.74 | 3.95 | 16.33 | 3.72 | 9.27 | 15.27 | 40.93 | 0.52 | 0.75 | 1.03 | 1.60 |
| Pharynx | 0.31 | 3.19 | 2.64 | 13.89 | 2.96 | 13.71 | 14.59 | 45.10 | 0.42 | 0.93 | 0.72 | 1.23 |
| Larynx | 0.36 | 1.32 | 1.22 | 6.70 | 2.87 | 8.37 | 7.20 | 21.81 | 0.50 | 0.63 | 0.68 | 1.23 |
| Total | 3.51 | 10.33 | 22.21 | 55.05 | 38.09 | 76.73 | 168.14 | 256.01 | 0.37 | 0.54 | 0.53 | 0.86 |
| Ratio+ (%) | 6.4 | 18.8 | 40.3 | 100 | 22.7 | 30.0 | 65.7 | 100 | 43.0 | 62.8 | 61.6 | 100 |

*V&V (vestibule and valve region), TR (turbinate region), NP (nasopharynx).
‡Effective diameter $d_e = 4V/A$.
+Ratio: the ratio of anatomical parameter to that of the adult.

**TABLE 4. Nostrils and upper trachea dimension of the four airway models of different ages.**

| Anatomy* | Coronal area, $A$ (mm$^2$) | | | | Perimeter, $P$ (mm) | | | | Hydr. diam., $d_h$‡ (mm) | | | |
|---|---|---|---|---|---|---|---|---|---|---|---|---|
| | 10 day | 7 month | 5 year | Adult | 10 day | 7 month | 5 year | Adult | 10 day | 7 month | 5 year | Adult |
| R nostril | 16.59 | 27.98 | 49.20 | 101.27 | 14.46 | 19.92 | 25.61 | 44.53 | 4.59 | 5.62 | 7.68 | 9.10 |
| L nostril | 16.59 | 31.48 | 43.74 | 101.27 | 14.46 | 20.49 | 24.89 | 44.53 | 4.59 | 6.15 | 7.03 | 9.10 |
| Trachea | 17.77 | 50.64 | 83.23 | 148.66 | 15.33 | 25.59 | 33.59 | 45.66 | 4.64 | 8.01 | 9.91 | 13.02 |

‡Hydraulic diameter $d_h = 4A/P$.

wall were tracked using a well-tested near-wall interpolation (NWI) algorithm proposed by Longest and Xi.[43]

To establish grid-independent and particle-count-independent results, convergence sensitivity analysis has been conducted following the method of Xi *et al.*[77] The final grid for reporting flow field and deposition conditions consisted of approximately 1.5–1.8 million cells with a thin five-layer pentahedral grid in the near-wall region and a first near-wall cell height of 0.05 mm. The final number of particles tracked was 60,000.

## RESULTS

### Infant–Child–Adult Discrepancy

The airway differences among the four subjects (i.e., 10-day-old neonate, the 7-month-old girl, the 5-year-old boy and the 53-year-old male) are apparent both in morphology and dimension. As for the morphology, younger subjects have smaller sized nostrils, shorter TRs, slender NP, and thinner pharynx–larynx. Moreover, the nostril shape appears circular at birth, becomes more oval during infancy and childhood, and eventually evolves into a wedge shape in adults (Fig. 2). Of particular interest are the TRs that appear undeveloped in both newborn and infant and are much simpler in morphology compared to those of the child and adult. The inferior meatus is missing in the

newborn. The inferior and middle meatuses grow with age both in size and complexity, as shown in Figs. 2a–2d. It is also noted that the angle of the pharynx in the 7-month-old infant is larger than others, preassembly due to a more back-tilted head position during image acquisition.

A quantitative comparison of airway dimensions among these four subjects is shown in Fig. 3 in terms of coronal cross-sectional area, perimeter, and hydraulic diameters, all as a function of distance from the nose tip. Comparison of airway volume and surface area among the four subjects in different anatomic sections are listed in Table 3. The dimension of two nostrils (i.e., inlets) and upper trachea (i.e., outlet) are shown in Table 4. From Table 3, the nasal–laryngeal airway volume of the 10-day newborn, the 7-month infant and the 5-year-old child is 6.4, 18.8, and 40.3% that of the adult, respectively. The nasal–laryngeal airway surface area of the newborn, infant and child is 22.7, 30.0, and 65.7% that of the adult, respectively. In particular, two major disparities are noted. First, for the three young subjects, each possesses a much narrower and smaller NP lumen compared to that of the adult. From Fig. 3a, the NP cross-sectional area of the newborn ($A = 31$ mm$^2$), infant ($A = 78$ mm$^2$) and child ($A = 170$ mm$^2$) is only 6, 15, and 32% that of the adult ($A = 535$ mm$^2$), respectively. From Fig. 3c, the NP hydraulic diameter of the newborn ($d_h = 5.7$ mm), infant ($d_h = 8.1$ mm) and the child ($d_h = 12.2$ mm) is

## (a) Cross-sectional Area



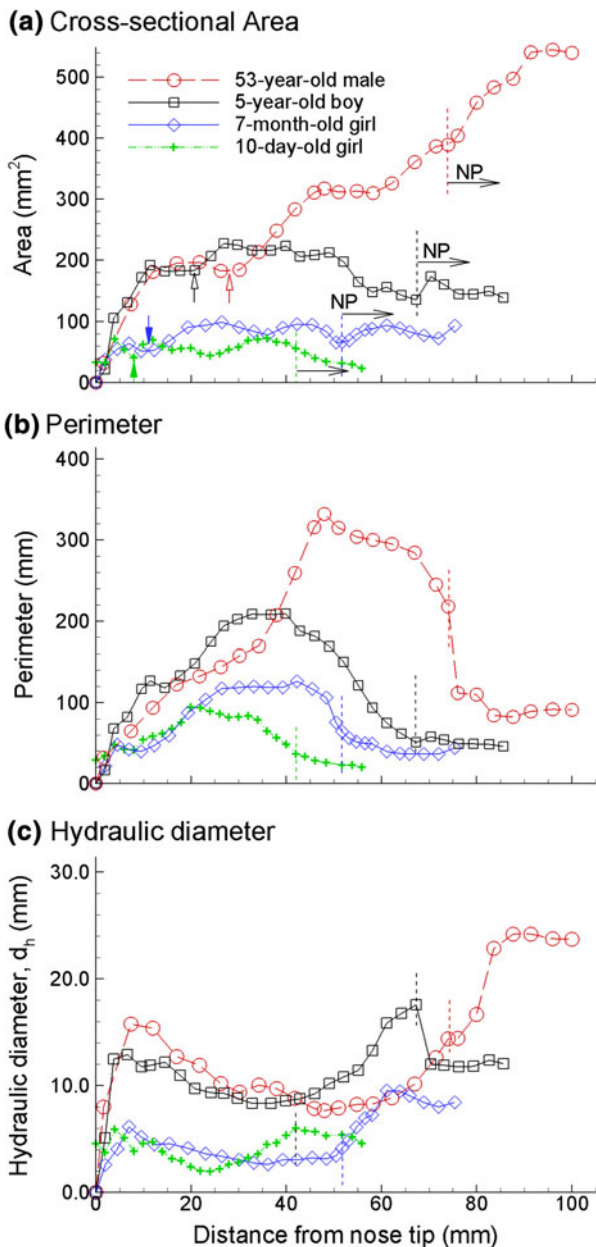## (b) Perimeter



## (c) Hydraulic diameter



FIGURE 3. Comparison of nasal dimensions among the neonate, infant, child, and adult as a function of the distance from the nose tip: (a) cross-sectional area, (b) perimeter, and (c) hydraulic diameter. The nasal valve (i.e., minimum cross-sectional area) is marked with an arrow in panel (a) for each model.

about one-fourth, one-third and half that of the adult (i.e., $d_h = 24.0$ mm), respectively. Secondly, the distance to the nasal valve (the minimum cross-sectional area) is much shorter in the newborn (8.0 mm, green solid arrow in Fig. 3a) and infant (11.2 mm, blue solid arrow) compared to the 5-year-old child (20.8 mm, black arrow) and adult (27.2 mm, red arrow). The nasal valve area is likewise smaller for the two youngest subjects (i.e., ~41.7 mm$^2$ for newborn and

~56 mm$^2$ for infant) compared to the child and adult (Fig. 3a).

### Breathing Resistance

The pressure differences across the nose–throat replica cast of the 5-year-old child are shown in Fig. 4a in comparison with numerical results in an identical computer airway model. The surface roughness of the cast is less than 0.1 mm and therefore negligible effect is expected on pressure drop from the roughness effect.[37,62,65] Good agreement was obtained between the measured and computed pressure drops for all the flow rates considered (i.e., 2–45 L/min), with the computed values being slightly larger than the measurement (<8%). Comparison of pressure drops among different ages is shown in Fig. 4b under quiet breathing conditions. It is noted that for an equivalent physical activity, the inhalation rates are different for different age groups due to their particular respiratory variables such as frequency, I:E ratio, and tidal volume, as listed in Table 2. Based on the elected flow rates (i.e., 3.8 L/min for 10-day girl, 6.5 L/min for 7-month girl, 11.2 for 5-year-old boy, and 18 L/min for adult), the nose–throat pressure drop is maximum for the 10-day newborn girl, and persistently decreases as age increases. Furthermore, this decrease appears most dramatic in the first year (10-day to 7-month herein), and the rate of decrease becomes gradually smaller beyond this age. Interestingly, a similar observation in respiratory rates was reported by Fleming *et al.*[22] who studied 3381 children and showed a constant decline in respiratory rate from birth to adolescence with the steepest fall in infants under 2 years of age, the possible linkage of which to breathing resistance will be discussed later. Besides age effects, the larger NP angle could also contribute to the dramatic decrease in pressure observed from the neonate to infant.

Figure 5 shows the nose–throat pressure drop (Δp) in the four subjects for a wide spectrum of breathing conditions in comparison to existing *in vitro* and *in vivo* measurements. *In vitro* data presented include an infant (9 month),[36] young children (1.5, 2.5, and 4 year),[13] and four adults.[25,37] *In vivo* data are from five adult subjects with an age range of 34 ± 5 year.[72] In general, the pressure drop (i.e., breathing resistance) decreases as the age increases. Infants and children have much higher breathing resistance than adults for a same flow rate. From Fig. 5, the pressure drop curve of the 10-day newborn agrees fairly well with the infant *in vitro* measurements, and that of the 5-year-old boy falls between those of young children and adults. However, our predicted resistances for the 7-month model are much lower compared to the *in vitro*
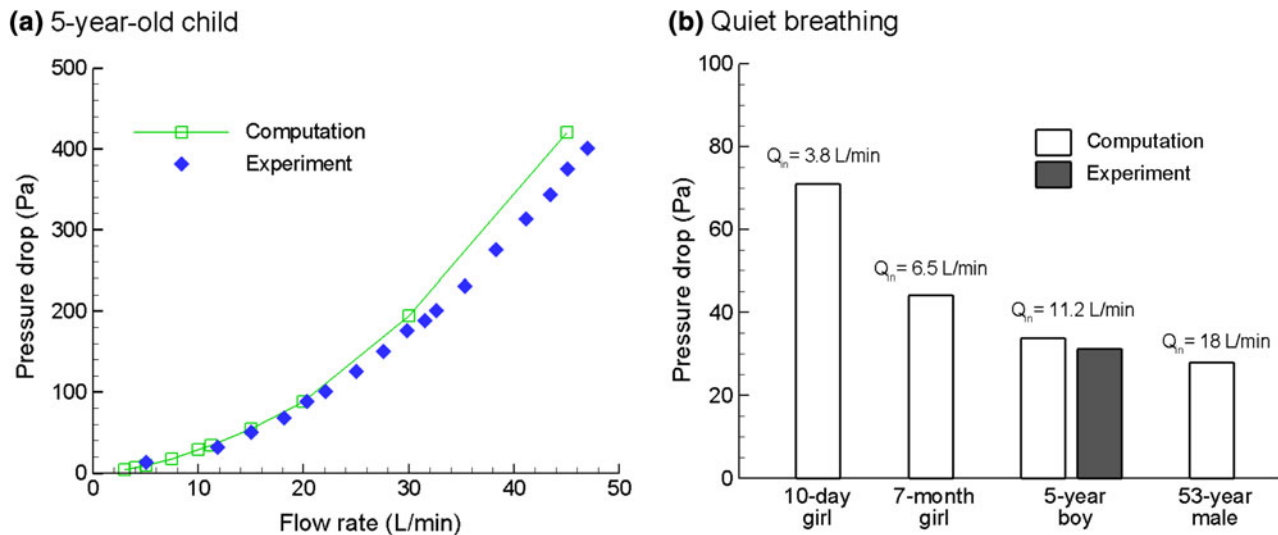
**(a)** 5-year-old child

**(b)** Quiet breathing

FIGURE 4. (a) Good agreement was achieved between predicted and measured pressure drops in the 5-year-child model. (b) Comparison of pressure drop predictions among the neonate, infant, child, and adult models under quiet breathing conditions.
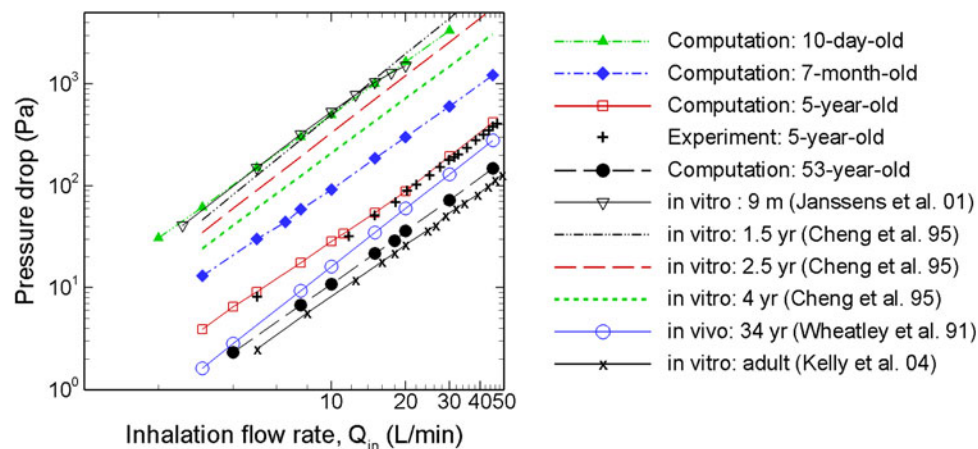
FIGURE 5. Nasal–laryngeal pressure drop (i.e., breathing resistance) as a function of inhalation flow rate (2–45 L/min) with comparison to *in vitro* and *in vivo* measurements in various age groups.

measurements in the infant groups (i.e., 9 m, 1.5 year, 2.5 year, as shown in Fig. 5). The pressure-flow relationships can be expressed as a power function ($\Delta P = aQ^b$), which can be plotted as straight lines on a log–log scale with slope "$b$". Table 5 lists the coefficients "$a$" and "$b$" for subjects of different ages. In light of the age-related effects, "$a$" constantly decreases in magnitude as age increases (from 5.86 for the newborn to 0.16–0.20 for adults).

### Airflow and Particle Deposition

Nasal airflows under quiet conditions in the newborn, infant, child, and adult are visualized in Fig. 6 as stream traces initiating at the right nostril of the four models considered. Flows of high velocity magnitude are observed in the middle portion of the nasal passages for all the four models considered. In contrast, the narrow fin-like meatus regions receive a minimal fraction of the airflow, especially in the deeper portions of each meatus. The main flow changes its direction dramatically from the nostrils to the NP, forming a nearly 180° curvature; however, this curvature is less severe for the 7-month infant model compared to the other three. No recirculation zone is observed in the NP of the three young subjects due to a much smaller airway diameter in this region, which is different from the adult NP where flow recirculation is obvious (Fig. 6a).

Particle depositions in the newborn, infant, child, and adult are compared in Figs. 6b and 6c under quiet breathing conditions for both small (1–10 nm) and large (20–100 nm) nanoparticles. Overall, more similarities than differences are observed among the four

TABLE 5. Pressure drop (i.e., breathing resistance) in nasal–laryngeal airways at different ages, $\Delta P(Pa) = aQ$ (L/min)$^b$.

| Age/reference | Method | $a^*$ | $b^*$ |
|---|---|---|---|
| 10 day, this study | CFD, CT model | 5.86 | 1.89 |
| 7 months, this study | CFD, CT model | 1.97 | 1.68 |
| 5 year, this study | CFD, MRI model | 0.58 | 1.70 |
| 5 year, this study | *In vitro*, MRI model | 0.42 | 1.77 |
| 53 year, this study | CFD, MRI model | 0.21 | 1.71 |
| 9 month (Saint), Janssens (01) | *In vitro*, CT cast | 8.87 | 1.75 |
| 1.5 year, Cheng (95) | *In vitro*, MRI cast | 5.24 ± 0.70 | 1.98 ± 0.060 |
| 2.5 year, Cheng (95) | *In vitro*, MRI cast | 4.46 ± 0.15 | 1.87 ± 0.014 |
| 4 year, Cheng (95) | *In vitro*, MRI cast | 3.40 ± 0.20 | 1.86 ± 0.023 |
| 34 ± 5 year, Wheatley (95) | *In vivo* | 0.20 ± 0.35 | 1.90 ± 0.028 |
| 53 year, Kelly (04) | *In vitro*, MRI cast (nose only) | 0.16 | 1.71 |
| Health 2, Garcia (09) | *In vitro*, MRI cast | 0.21 ± 0.016 | 1.78 ± 0.01 |
| Health 4, Garcia (09) | *In vitro*, MRI cast | 0.09 ± 0.013 | 1.85 ± 0.01 |
| Atrophic, Garcia (09) | *In vitro*, MRI cast | 0.04 ± 0.005 | 1.87 ± 0.02 |

models, with deposition patterns exhibiting much less heterogeneity than observed for micron particles.[77] As expected, a large portion of ultrafine aerosols in the range of 1–10 nm deposit in the nasal–laryngeal airways for all models considered, while only a small portion of 20–100 nm aerosols deposit due to the dramatically decreased diffusivity. In light of local depositions, 1–10 nm ultrafine aerosols accumulate either in TRs or pharynx–larynx region, while the larger nanoparticles (20–100 nm) accumulate mainly in the pharynx–larynx region where turbulence is most pronounced. One explanation for the ultrafine particle accumulation in the TR is the narrow airway channel with the high particle diffusivity that disperses ultrafine particles onto the turbinate walls. These particles will be either absorbed into capillary systems, or be moved to the NP by mucociliary transport and cleared out by cough or swallowing. Besides, the variation of deposition locations with inhalation flow rates was found not apparent.

To determine how accurately our modeling capture the dynamic mechanisms involved, current CFD results were compared with existing experimental data in comparable airway models for both infants[13,29] and adults[12,14,29] (Fig. 7). However, only *in vitro* models that possess closest geometric dimensions with current models were selected for validation purpose. For example, although there are three subjects considered in Cheng *et al.*[13] (i.e., 1.5, 2.5, and 4 year), only the 4-year-old one was selected to compare with the 5-year-old CFD data due to closest ages. The subjects selected from the study of Golshahi *et al.*[29] is Subject 1 (male, age unknown, volume: 52.338 cm$^3$, surface area: 284.44 cm$^2$) for adult comparison and Subject 8 (male, age 8 m, volume: 10.342 cm$^3$, surface area: 101.42 cm$^2$)[66] for infant comparison. Generally, good agreements are achieved between numerical predictions and *in vitro* measurements for the whole range of

ultrafine particles and for both adults and younger subjects. Specifically, the adult CFD airway model and the *in vitro* cast implemented in Cheng *et al.*[12] are based on the same set of MR images. Therefore, a direct comparison of deposition results between simulations and measurements is possible. From Fig. 7a, at an inhalation flow rate of 10 L/min, the simulation results agreed with Cheng *et al.*[12] data to a high degree. This gave us confidence that the numerical method employed in this study is adequate to capture the physical realisms of interest, and has been used to carry out a systemic numerical experiment addressing age-related effects under a wide range of inhalation scenarios as listed in Table 3.

Figure 8 shows the 3-D surface plot of the deposition fractions in the nasal–laryngeal airways of the four subjects as a function of both inhalation flow rate and particle size. The inhalation flow rates considered are 2, 3, 5, 7, 10, 15, 20, 30, 45 L/min and the particle sizes are in the range of 1–100 nm. The four surface plots look alike both in trend and magnitude, with declining deposition rate as the particle size and flow speed increase. The peak deposition rate occurs at the smallest particle size and lowest flow rate considered ($d_p = 1$ nm and $Q_{in} = 2$ L/min) where the Brownian motion and residence time of the particles are both maximal. However, the relative role of the convective (flow rate) and molecular (particle size) diffusion differs in the ultrafine aerosol deposition, as the effect of molecular diffusion apparently overweighs that of convection for the breathing conditions considered herein. Considering the larger nanoparticles in the range of 20–100 nm, very low deposition fractions are observed for all models considered.
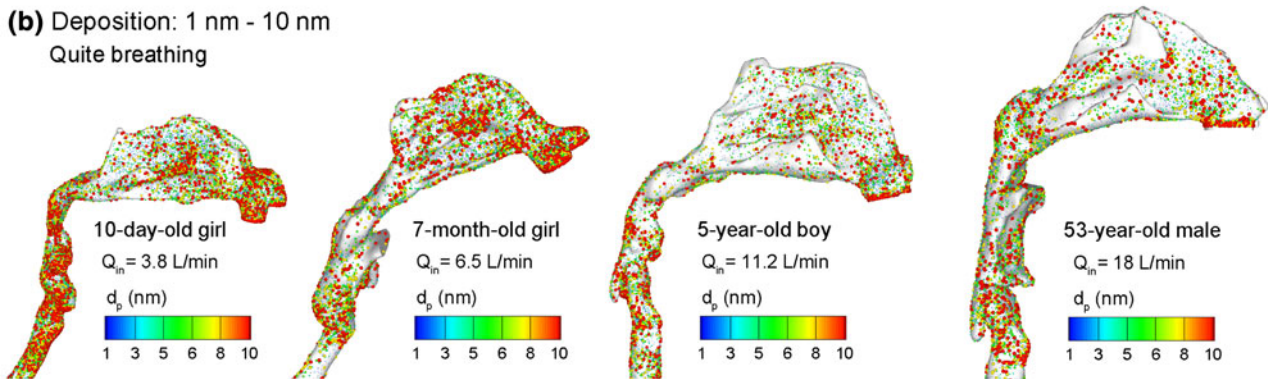
To further evaluate the predicted deposition results, the same data in Fig. 8 has been plotted as a function of two existing diffusion parameters proposed from *in vitro* and *in vivo* deposition studies (Fig. 9). The first

**(a) Streamtraces**
Quite breathing
Surafce 90% transparent
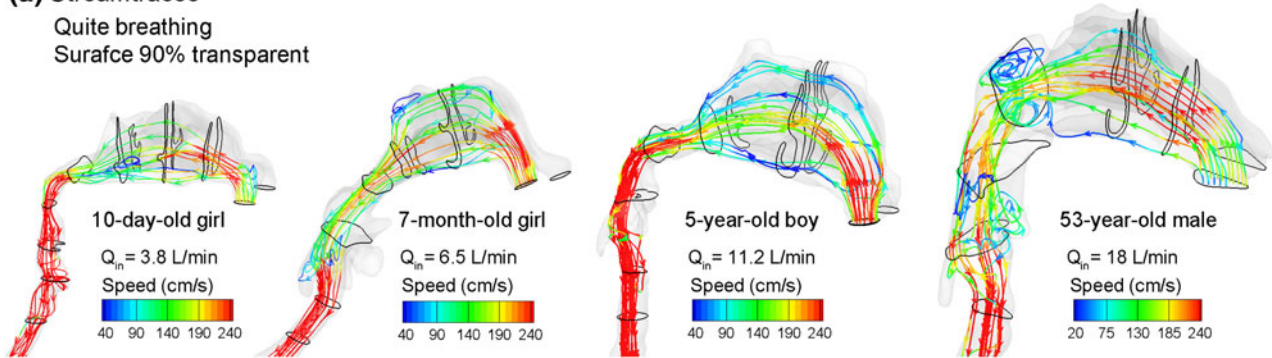


**(b) Deposition: 1 nm - 10 nm**
Quite breathing



**(c) Deposition: 20 nm - 100 nm**
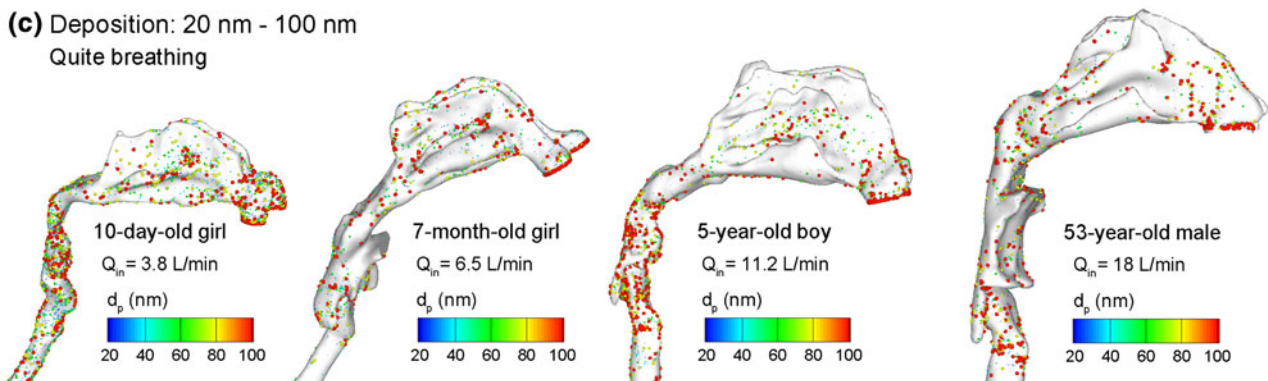Quite breathing



FIGURE 6. Comparison of (a) airflow streamtraces and aerosol depositions for nanoparticles of (b) 1–10 nm and (c) 20–100 nm.

parameter ($D^{0.5}Q^{-0.125}$) was theoretically derived by Cheng et al.[15] based on the assumption of turbulent diffusion in pipe flow and was later adopted in a series of in vitro replica studies.[12,14,16] The second parameter ($D^{0.5}Q^{-0.28}$) was later derived by Cheng et al.[12] based on in vivo deposition data, which exhibited a greater dependence on flow rate (i.e., exponent of −0.28) than the replica-based parameter (i.e., exponent of −0.125). Figures 9a and 9b compare the deposition profiles plotted as a function of the above two diffusion parameters in the 5-year-old model. From Fig. 9a, it is noted that the deposition results do not fully collapse for different flow rates and particle sizes, suggesting that the replica-based parameter ($D^{0.5}Q^{-0.125}$) does not

accurately account for the relative effect from convection and diffusion. In contrast, a more precise correlation was obtained by plotting the results as a function of the in vivo-based parameter ($D^{0.5}Q^{-0.28}$). Following the format of the in vivo empirical correlation suggested by Cheng et al.,[12] $DF = 1 - \exp(-aD^{0.5}Q^{-0.28})$, a coefficient of $a = 12.5$ was obtained for the 5-year-old deposition results (Fig. 9b). The resulting $R^2$ value was 0.93, indicating reasonably good agreement between the numerical data and the proposed empirical correlation. However, deviation becomes noticeable from $D^{0.5}Q^{-0.28} = 0.11$ and aggravates thereafter. Considering that deposition in the diffusion regime was also affected by non-continuum
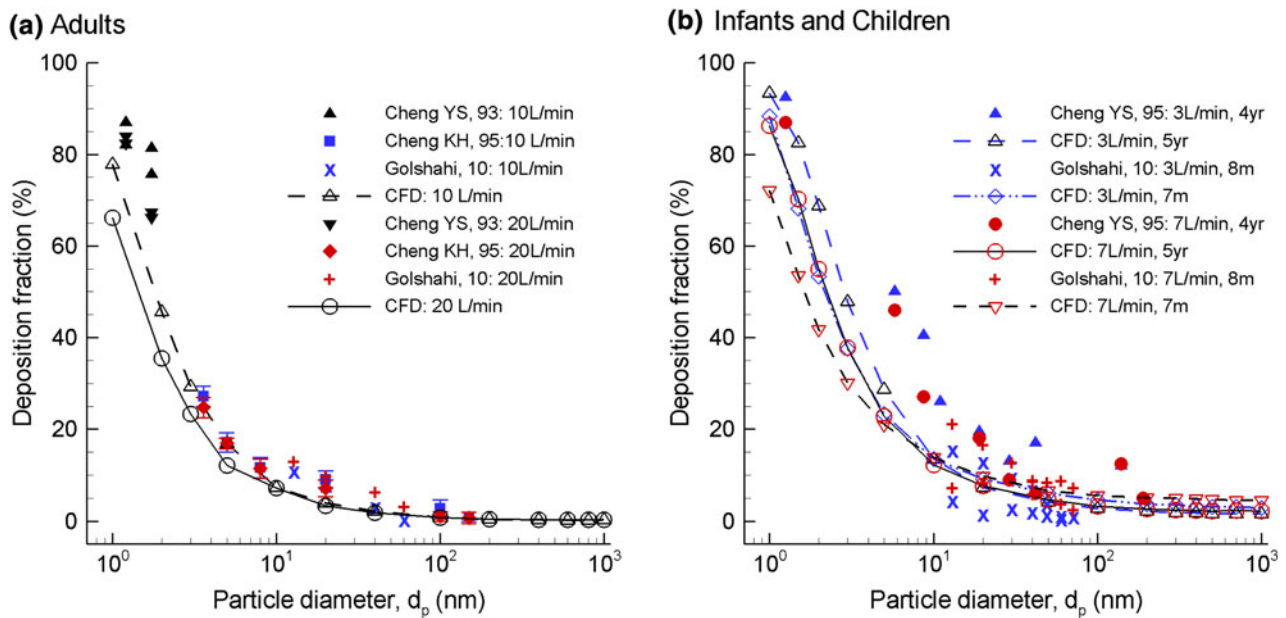
**FIGURE 7.** A comparison between numerically predicted depositions and existing *in vitro* measurements among airway models with similar dimensions. (a) Adults and (b) infants and children. Considering the adults case, the two models in CFD and Cheng KH, 95 were developed from an identical set of MRI data, between which excellent agreement was also obtained.

effects, the Cunningham correction factor $C_c$ was incorporated into the diffusion parameter as $(C_c^b D^{0.5} Q^{-0.28})$.[12] Again, an equation of $\mathrm{DF} = 1 - \exp(-c C_c^b D^{0.5} Q^{-0.28})$ was used to fit the expiratory simulation data. The best-fit values of $b$ and $c$ were 0.25 and 3.5, respectively, resulting in $R^2 = 0.98$ (Fig. 9b). The resulting ultrafine regime correlation in the nasal–laryngeal airways for the 5-year-old child model is expressed as

$$\text{5-year-old child: } \mathrm{DF} = 1 - \exp\left(-3.5 C_c^{0.25} D^{0.5} Q^{-0.28}\right) \tag{2}$$

As evident from Figs. 9a and 9, inclusion of the Cunningham correction factor results in a better approximation of the numerical data in comparison to the *in vivo*-based correlation (Fig. 9b), and represents a significant improvement over the replica-based profile in Fig. 9a.

Figure 9c shows the predicted deposition results as a function of $D^{0.5} Q^{-0.28}$ for the 7-month infant. The 5-year-old child deposition data are also superimposed to emphasize the age-related effects. Likewise, better approximations are obtained by including the Cunningham factor for the deposition results of the 7-month infant, which is expressed as

$$\text{7-month-old infant: } \mathrm{DF} = 1 - \exp\left(-3.9 C_c^{0.17} D^{0.5} Q^{-0.28}\right) \tag{3}$$

Comparison of depositions among the four subjects as a function of $D^{0.5} Q^{-0.28}$ is shown in Fig. 9d. For a given value of diffusion factor ($D^{0.5} Q^{-0.28}$), the deposition results of the newborn and infant fall below those of the child and adult. Moreover, results of the child and adult appear to collapse into one single curve. As such, the correlation (Eq. 2) for the child is also applied to the 53-year-old adult model in this study. The newborn deposition data lie slightly beneath that of the 7-month-old infant, but are very close. Therefore, the correlation in Eq. (3) can also be applied to approximate ultrafine depositions for subjects aged below 7 month. Furthermore, these two correlations can also be applied to depositions of gases and vapors in the nasal–laryngeal airway for cases of rapid absorption on the airway surface.

### Sub-regional and Local Depositions

Comparison of sub-regional deposition among the four subjects is shown in Fig. 10 for varying particle sizes and a flow rate of 15 L/min. The sub-regions considered include nasal V&V, TR, NP, pharynx, and larynx, as illustrated in Fig. 2. In light of age effects, one observation hereof is noteworthy: the deposition partitions among the four sub-regions (i.e., turbinate, NP, pharynx, and larynx) are different among the four airway models considered. For example, in the TR, the 5-year-old child model receives the highest deposition while the 10-day newborn model receives the least for all particle sizes and flow rates considered (Fig. 10a). While in the larynx, the 5-year-old model receives less than the other three models. Mechanisms behind these
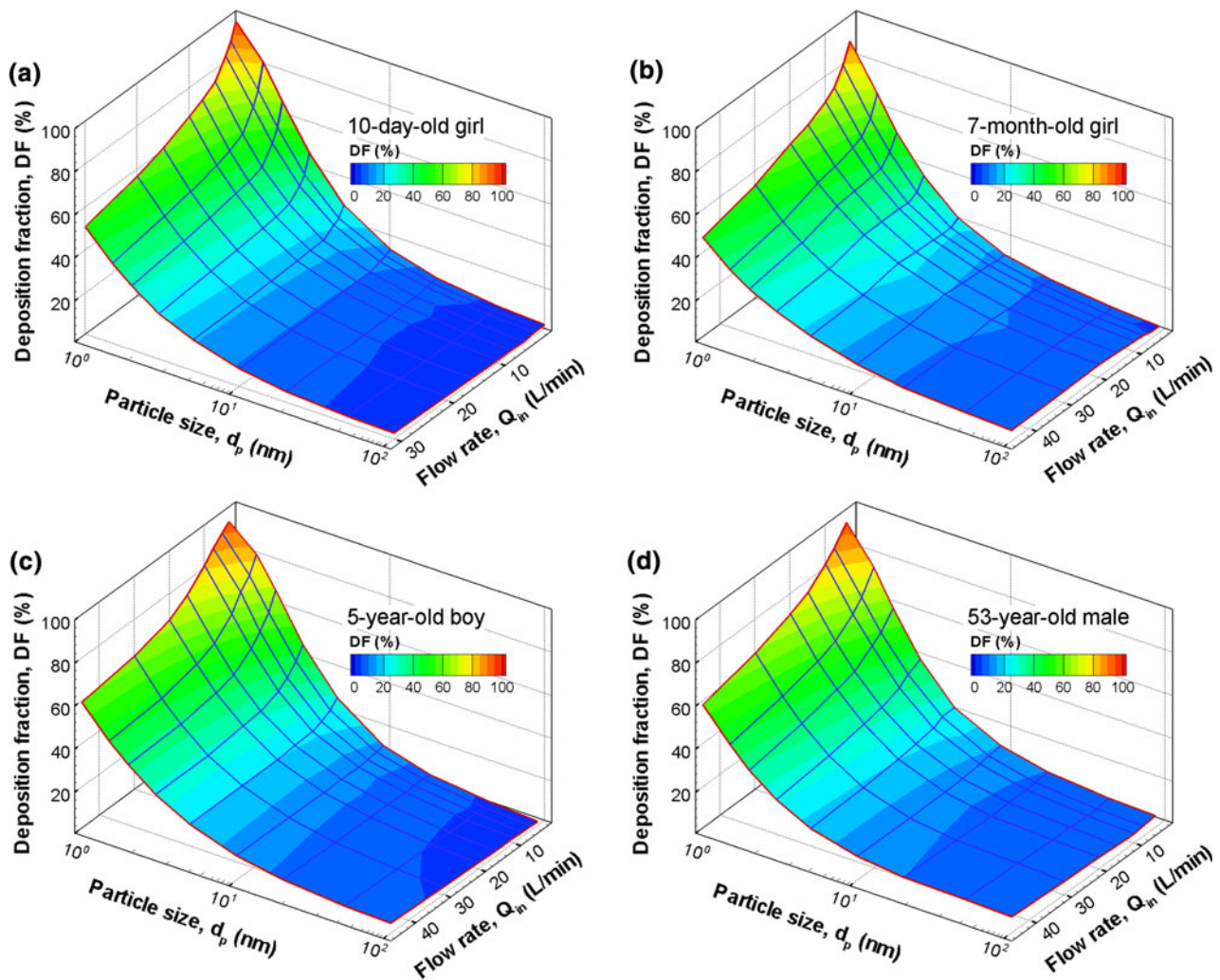
FIGURE 8. 3-D surface plot of the total deposition fractions as a function of particle diameter and inhalation flow rate among the (a) 10-day-old girl, (b) 7-month-old girl, (c) 5-year-old boy, and (d) 53-year-old male.

irregular partitions could be complex, such as turbulent dispersion, secondary motion, particle depletion in upstream regions, etc. However, this finding is worthy of our further attention. For inhalation toxicology, it may suggest a different burden on the region of interest among subjects of different ages. Meanwhile, for inhalation therapy that targets drugs at designated site of the respiratory system, this finding may imply that existing adult deposition results might not guarantee an accurate dose planning for pediatric patients.

To highlight the age-related effects on microdosimetry, a comparison of local deposition enhancement factor (DEF) values among the newborn, infant, child, and adult is illustrated in Fig. 11 for particles of 5 nm and quiet breathing conditions. By definition, the DEF value quantifies the particle dosage over an area of 50 airway epithelial cells in length with respect to the average deposition rate. As discussed, highest DEF values are observed in the adult model ($DEF_{max} = 37$)

that possesses the most sophisticated structures, while lowest $DEF_{max}$ values are found in the 10-day-old newborn model that has most primitive respiratory anatomy ($DEF_{max} = 22$). Albeit these slight variations, the $DEF_{max}$ values among the four models are of the same order of magnitude, i.e., 22–37. This is in contrast with the much elevated DEF values observed in the case of micron aerosols in the 5-year-old child model,[77] which is more than one order of magnitude higher (i.e., $DEF_{max} = 830$ for 10 $\mu$m particles and 10 L/min flow rate) than the DEF values as observed here for nanoparticles. The overall pattern of deposition enhancement appears very similar for these four models. Each model exhibits hot spots on the dorsal walls of the larynx where convective diffusion is high due to converging airflow to the narrow glottis. Other hot spots with less elevated DEF values are observed in the TR for each model. It is also noted that the nasal valve and pharyngeal dorsal wall do not have significant
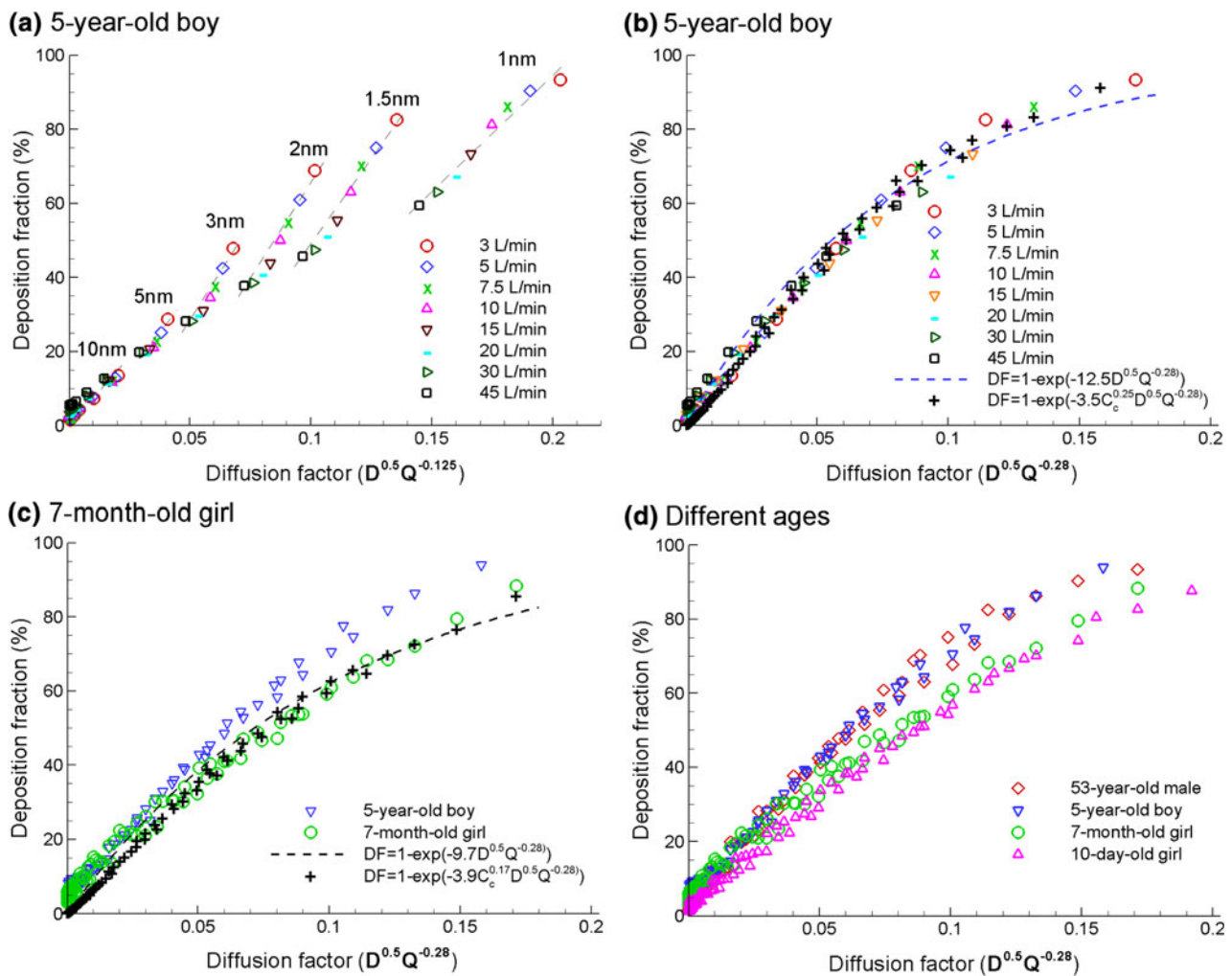
**FIGURE 9.** Comparison of the deposition fractions as a function of the diffusion factor based on existing (a) *in vitro* ($D^{0.5}Q^{-0.125}$) and (b) *in vivo* ($D^{0.5}Q^{-0.28}$) studies in the 5-year-old child model. Inclusion of the Cunningham correction factor ($C_c$) further improves agreement between the correlation and numerical data (b). Comparison of deposition fractions among the four models as a function of $D^{0.5}Q^{-0.28}$ are shown in (c) and (d). Units: $Q$ (L/min) and $D$ (cm²/s).

hot spots, which was the case for 10 $\mu$m aerosols.[77] This lack of hot spots in the valve and pharynx regions is due to the negligible inertial impaction effect for ultrafine particles which can closely follow the main flow and easily maneuver through the constricted or highly curved passages.

## DISCUSSION

Infancy and childhood are periods of enormous physiological changes, particularly in the early months and years. Significant differences were noted of the nose–throat anatomy among the four subjects of different ages, i.e., a newborn, an infant, a child, and an adult. These differences manifest themselves not only in airway dimension but also in airway morphology. For example, the nasal–laryngeal airway volume of the

10-day-old neonate, the 7-month-old infant, and the 5-year-old child is 6.4, 18.8, and 40.3% that of the adult, respectively. At the same time, the three young subjects have smaller sized nostrils, a shorter TR, and a much slender NP. Results of this study indicate that the nasal valve and vestibule region might mature around the age of five. This is supported by the much shorter nostril-valve distance (i.e., 8.0 and 11.2 mm for newborn and infant vs. 20.8 and 27.2 mm for child and adult, respectively) and much smaller valve cross-sectional area in the 10-day newborn and 7-month infant compared to the 5-year-old child and adult (i.e., 42 and 56 mm² for newborn and infant vs. ~180 mm² for child and adult) (Fig. 3). The TR experiences fast growth from birth to the age of five as indicated by the remarkable volume increase of this region in Table 3 (i.e., 1.57 cm³ for newborn, 2.83 cm³ for infant, 11.03 cm³ for child, and 12.63 cm³ for adult); however,
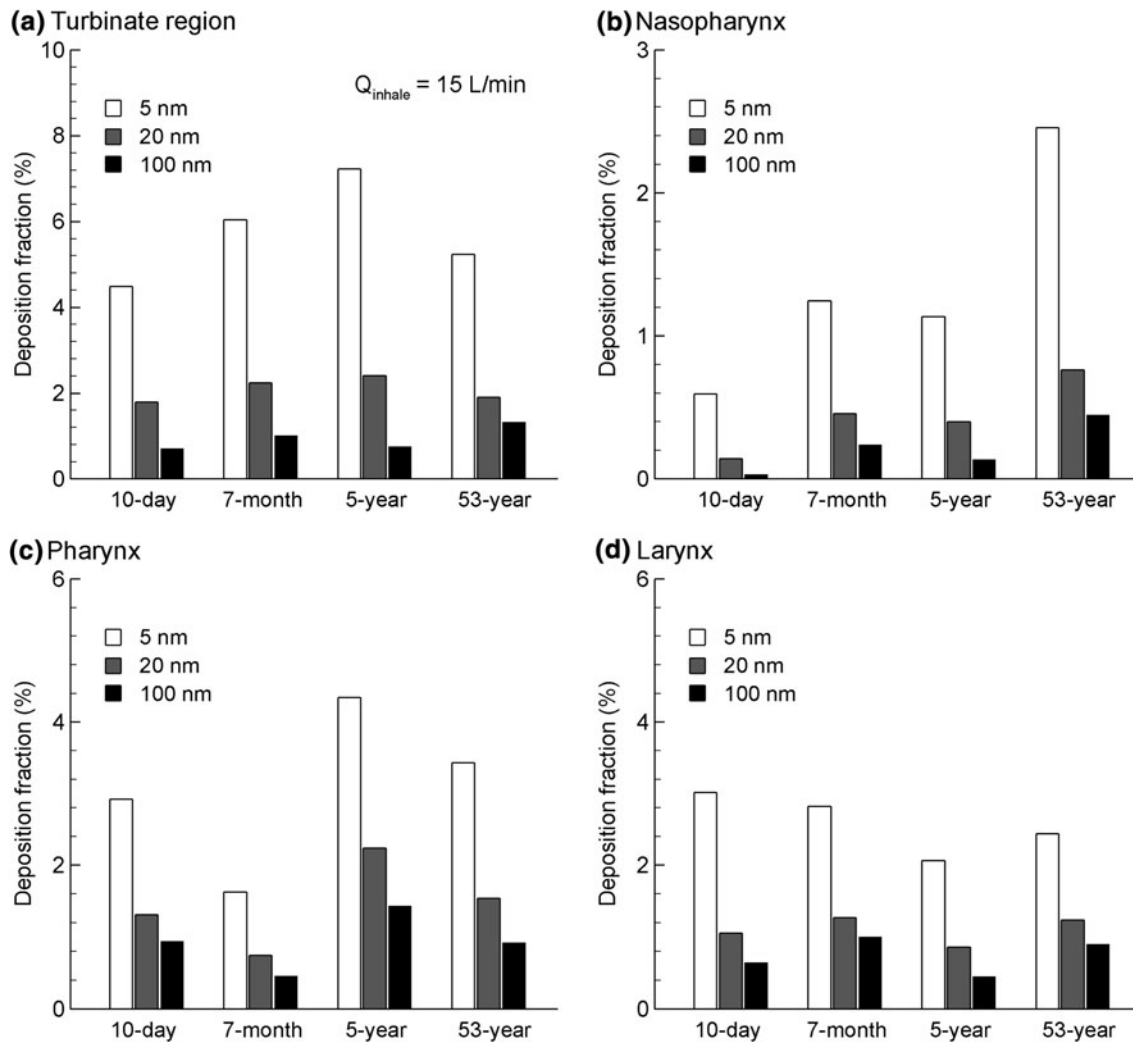
**FIGURE 10.** Comparison of sub-regional deposition fractions among the four models (10-day, 7-month, 5-year, and 53-year) for different particle sizes (5, 20, and 100 nm) at the site of (a) turbinate region, (b) nasopharynx, (c) pharynx, and (d) larynx.

a lack of similarity in shape between the 5-year-old child and adult may still mean an undeveloped turbinate in the child. It is apparent that the NP grows the least during the first five years (i.e., volume = 0.48 cm$^3$ for newborn, 1.74 cm$^3$ for infant, 3.95 cm$^3$ for child, and 16.33 cm$^3$ for adult; Table 3). Further studies on specific age groups are necessary to quantify the developmental physiology and their associated effects on breathing and aerosol filtrations.

By implementing the flow-resistance equation $\Delta P = aQ^b$, the base value "$a$" and exponent "$b$" were identified for subjects at different ages from both experimental (*in vivo* and *in vitro*) and computational data (Table 5). As discussed before, for a same ventilation flow rate, younger subjects experience much higher resistances. It is therefore reasonable that the magnitude of "$a$", which dictates the resistance magnitude, persistently decreases with age (from 8.87 for 10-day newborn to 0.16–0.54 for adult). The magnitude

of "$b$" (i.e., slope of the $\Delta p - Q_{in}$ curve) means the sensitivity level of breathing resistance to the ventilation level (or physical activity level). In this study, the magnitudes of "$b$" for different age groups are close in range ($b = 1.71$–$1.98$), indicating similar flow-resistance sensitivities from birth to adulthood. Furthermore, the exponent "$b$" is positive and larger than one, indicating that the breathing resistance increases dramatically as the minute ventilation rate increases. Children breathe at a higher frequency than adults. The mechanism that regulates such respiratory rates is, however, still not fully known.[22] For example, Mortola[51] observed that in newborns at higher ventilation levels, only the respiratory frequency increases while the tidal volume remains largely the same. Considering the fundamental mechanism that a combination of tidal volume and respiratory rate be spontaneously elected that minimizes the breathing energy, the finding in this study might lend some hints to the above observation.
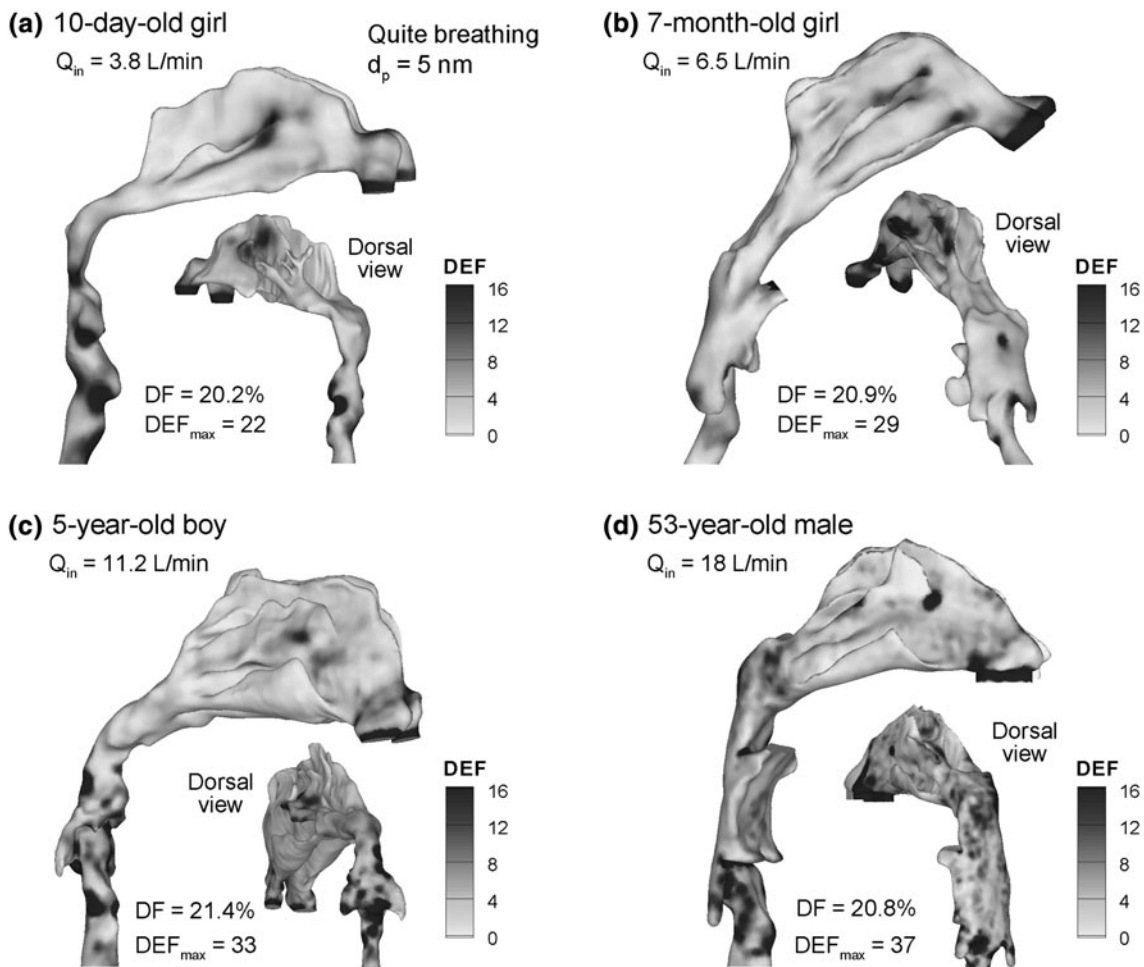
**FIGURE 11.** Comparison of the microdosimetry (i.e., local deposition enhancement factors, or DEF) under quite breathing conditions and $d_p$ = 5 nm in the airway models of (a) 10-day-old girl, (b) 7-month-old girl, (c) 5-year-old boy, and (d) 53-year-old male.

Because of the dramatic flow-resistance relation ($b = \sim2$), increasing respiratory frequency instead of tidal volume (i.e., much higher resistance) is probably an energy-saving strategy of newborns to cope with higher physical activities.

Respiratory disorders are diverse both in etiology and manifestations. Knowing detailed deposition information is usually fundamental to the identification of causality and assessment of dose-outcome response. The sub-regional and localized deposition values herein, which are amongst the first studies characterizing the detailed depositions in neonates, infants and children, have implications in narrowing down or pinpointing the site of highest possibility (SHP) for respiratory lesions in infants and children. These deposition hot spots are most susceptible to cancer formation, and are therefore extremely important to identify. In this study, the deposition hot spots are observed mainly on the turbinate as well as the dorsal wall of the larynx. Besides, the deposition partition in sub-regions (i.e., turbinate, NP, pharynx, and

larynx) is quite different among the four age groups considered, indicating a different level of burdens upon the region of interest even when exposed to the same environment. From the drug delivery perspective, this difference implies that existing adult deposition results might not guarantee an accurate dose planning for children and infants.

While multiple empirical correlations of nanoparticle depositions exist for adults and to a lesser extent for children, correlations including age effects are still rare. A significant issue in accounting for age effects is to determine the appropriate parameter that best represents the variations of nasal–laryngeal morphology and dimension with age. This parameter could be biological data such as age, height, weight, head circumference, respiratory rate, or nasal–laryngeal airway data itself such as volume, surface area, hydraulic diameter, or transnasal pressure drop which has been adopted to collapse intersubject variability for inertial depositions.[25,39,59,66] Even though a single correlation applicable to all age groups is highly desirable, such a

correlation has to be awaited until more nasal morphology and deposition data become available for subjects of a large spectrum of ages. It is also a reminder (or caution) that there exist multiple ways in presenting/comparing/extrapolating deposition data in light of the age effects. For instance, besides the physical activity condition as in this study, deposition rates have also been compared in terms of ventilation rate,[3] per airway surface area,[19] and per body mass[56] depending on their comparison purpose. Considering the fact that terminologies defining the ventilation level are relatively arbitrary as no standard definitions exist,[57] comparing data from different studies is often not straightforward.

Limitations of this study include the assumptions of steady flow, simplified inlet conditions, rigid airway walls, idealized particles, and limited number of samples per age group. Other studies have highlighted the physical significance of tidal breathing,[33,55] inlet velocity profiles,[67] airway wall motion,[23,55] nasal valve collapse [8,9] and glottal aperture variation.[7,76] Besides, almost all environmental ultrafine aerosols are non-spherical,[34,70] interacting,[52] and some may undergo changes in size due to hygroscopic effect,[44] or coagulation.[53] Moreover, each model in this study is based on images of one single subject and does not account for the intersubject variability which can be significant.[25,29,31,45,58,66] Another limitation is the typical supine position of the subjects during data acquisition, which is different from sedentary breathing. Images acquired at the end of the inhalation may not reflect variations in airway geometry during a full breathing cycle. Therefore, future studies are needed that should be orientated toward: (1) improving physical realism and (2) including a broader population group. Our knowledge of nasal deposition is currently lacking in subpopulations such as pediatrics, geriatrics, and patients with respiratory diseases. Due to physiological development, aging, or diseases states, the airway anatomy can be remarkably different from that of a healthy adult. Concentrating on these specific subpopulations will help to clarify inter-group and inter-individual variability and will allow for the design of more efficient pharmaceutical formulations and drug delivery protocols for different age groups.

## CONFLICT OF INTEREST

None.

## REFERENCES

[1]Allen, M. D., and O. G. Raabe. Slip correction measurements of spherical solid aerosol particles in an improved Millikan apparatus. *Aerosol Sci. Technol.* 4:269–286, 1985.

[2]Asgharian, B., M. G. Ménache, and F. J. Miller. Modeling age-related particle deposition in humans. *J. Aerosol Med.* 17(3):213–224, 2004.

[3]Becquemin, M. H., D. L. Swift, A. Bouchikhi, M. Roy, and A. Teillac. Particle deposition and resistance in the noses of adults and children. *Eur. Respir. J.* 4(6):694–702, 1991.

[4]Bennett, W. D., and K. L. Zeman. Effect of race on fine particle deposition for oral and nasal breathing. *Inhalation Toxicol.* 17(12):641–648, 2005.

[5]Bennett, W. D., K. L. Zeman, and A. M. Jarabek. Nasal contribution to breathing and fine particle deposition in children versus adults. *J. Toxicol. Environ. Health Part A* 71(3):227–237, 2008.

[6]Bobak, M., and D. A. Leon. The effect of air pollution on infant mortality appears specific for respiratory causes in the postneonatal period. *Epidemiology* 10(6):666–670, 1999.

[7]Brancatisano, T., P. W. Collett, and L. A. Engel. Respiratory movements of the vocal cords. *J. Appl. Physiol.* 54(4):1269–1276, 1983.

[8]Bridger, G. P. Physiology of the nasal valve. *Arch. Otolaryngol. Head Neck Surg.* 92(6):543–553, 1970.

[9]Bridger, G. P., and D. F. Proctor. Maximum nasal inspiratory flow and nasal resistance. *Ann. Otol. Rhinol. Laryngol.* 79(3):481–488, 1970.

[10]Cheng, Y. S. Aerosol deposition in the extrathoracic region. *Aerosol Sci. Technol.* 37:659–671, 2003.

[11]Cheng, K. H., Y. S. Cheng, H. C. Yeh, R. A. Guilmette, S. Q. Simpson, S. Q. Yang, and D. L. Swift. In vivo measurements of nasal airway dimensions and ultrafine aerosol depositing in human nasal and oral airways. *J. Aerosol Sci.* 27:785–801, 1996.

[12]Cheng, K. H., Y. S. Cheng, H. C. Yeh, and D. L. Swift. Deposition of ultrafine aerosols in the head airways during natural breathing and during simulated breath holding using replicate human upper airway casts. *Aerosol Sci. Technol.* 23(3):465–474, 1995.

[13]Cheng, Y. S., S. M. Smith, H. C. Yeh, D. B. Kim, K. H. Cheng, and D. L. Swift. Deposition of ultrafine aerosols and thoron progeny in peplicas of nasal airways of young children. *Aerosol Sci. Technol.* 23(4):541–552, 1995.

[14]Cheng, Y. S., Y. F. Su, H. C. Yeh, and D. L. Swift. Deposition of Thoron progeny in human head airways. *Aerosol Sci. Technol.* 18:359–375, 1993.

[15]Cheng, Y. S., Y. Yamada, H. C. Yeh, and D. L. Swift. Diffusional deposition of ultrafine aerosols in a human nasal cast. *J. Aerosol Sci.* 19:741, 1988.

[16]Cheng, Y. S., H. C. Yeh, R. A. Guilmette, S. Q. Simpson, K. H. Cheng, and D. L. Swift. Nasal deposition of ultrafine particles in human volunteers and its relationship to airway geometry. *Aerosol Sci. Technol.* 25(3):274–291, 1996.

[17]Cohen Hubal, E. A., J. S. Kimbell, and P. S. Fedkiw. Incorporation of nasal-lining mass-transfer resistance into a CFD model for prediction of ozone dosimetry in the upper respiratory tract. *Inhalation Toxicol.* 8(9):831–857, 1996.

[18]Crawford, D. J. Identifying critical human subpopulations by age groups: radioactivity and the lung. *Phys. Med. Biol.* 27:539–552, 1982.

[19]Diot, P., L. B. Palmer, A. Smaldone, J. Decelie-Germana, R. Grimson, and G. C. Smaldone. RhDNase I aerosol deposition and related factors in cystic fibrosis. *Am. J. Respir. Crit. Care Med.* 156(5):1662–1668, 1997.

[20]Everard, M. L. Inhalation therapy for infants. *Adv. Drug Deliv. Rev.* 55(7):869–878, 2003.

[21]Faustman, E. M., S. M. Silbernagel, R. A. Fenske, T. M. Burbacher, and R. A. Ponce. Mechanisms underlying children's susceptibility to environmental toxicants. *Environ. Health Perspect.* 108:13–21, 2000.

[22]Fleming, S., M. Thompson, R. Stevens, C. Heneghan, A. Plüddemann, I. Maconochie, L. Tarassenko, and D. Mant. Normal ranges of heart rate and respiratory rate in children from birth to 18 years of age: a systematic review of observational studies. *Lancet* 377(9770):1011–1018, 2011.

[23]Fodil, R., L. Brugel-Ribere, C. Croce, G. Sbirlea-Apiou, C. Larger, J. F. Papon, C. Delclaux, A. Coste, D. Isabey, and B. Louis. Inspiratory flow in the nose: a model coupling flow and vasoerectile tissue distensibility. *J. Appl. Physiol.* 98(1):288–295, 2005.

[24]Gagliardi, L., F. Rusconi, M. Castagneto, G. L. N. Porta, S. Razon, and A. Pellegatta. Respiratory rate and body mass in the first three years of life. *Arch. Dis. Child.* 76(2):151–154, 1997.

[25]Garcia, G. J. M., E. W. Tewksbury, B. A. Wong, and J. S. Kimbell. Interindividual variability in nasal filtration as a function of nasal cavity geometry. *J. Aerosol Med. Pulm. Drug Deliv.* 22(2):139–155, 2009.

[26]Ghalati, P. F., E. Keshavarzian, O. Abouali, A. Faramarzi, J. Y. Tu, and A. Shakibafard. Numerical analysis of micro- and nano-particle deposition in a realistic human upper airway. *Comput. Biol. Med.* 42(1):39–49, 2012.

[27]Ginsberg, G., B. Foos, R. B. Dzubow, and M. Firestone. Options for incorporating children's inhaled dose into human health risk assessment. *Inhalation Toxicol.* 22(8):627–647, 2010.

[28]Ginsberg, G. L., B. P. Foos, and M. P. Firestone. Review and analysis of inhalation dosimetry methods for application to children's risk assessment. *J. Toxicol. Environ. Health Part A* 68(8):573–615, 2005.

[29]Golshahi, L., W. H. Finlay, J. S. Olfert, R. B. Thompson, and M. L. Noga. Deposition of inhaled ultrafine aerosols in replicas of nasal airways of infants. *Aerosol Sci. Technol.* 44(9):741–752, 2010.

[30]Gradon, L., and C. P. Yu. Diffusional particle deposition in the human nose and mouth. *Aerosol Sci. Technol.* 11:213–220, 1989.

[31]Grgic, B., W. H. Finlay, P. K. P. Burnell, and A. F. Heenan. In vitro intersubject and intrasubject deposition measurements in realistic mouth-throat geometries. *J. Aerosol Sci.* 35(8):1025–1040, 2004.

[32]Guilmette, R. A., Y. S. Cheng, H. C. Yeh, and D. L. Swift. Deposition of 0.005–12 micrometer monodisperse particles in a computer-milled, MRI-based nasal airway replica. *Inhalation Toxicology* 6(Suppl. 1):395–399, 1994.

[33]Haussermann, S., A. G. Bailey, M. R. Bailey, G. Etherington, and M. Youngman. The influence of breathing patterns on particle deposition in a nasal replicate cast. *J. Aerosol Sci.* 33(6):923–933, 2002.

[34]Inthavong, K., H. Wen, Z. F. Tian, and J. Y. Tu. Numerical study of fibre deposition in a human nasal cavity. *J. Aerosol Sci.* 39(3):253–265, 2008.

[35]Inthavong, K., K. Zhang, and J. Y. Tu. Numerical modelling of nanoparticle deposition in the nasal cavity and the tracheobronchial airway. *Comput. Methods Biomech. Biomed. Eng.* 14(7):633–643, 2011.

[36]Janssens, H. M., J. C. de Jongste, W. J. Fokkens, S. G. Robben, K. Wouters, and H. A. Tiddens. The Sophia Anatomical Infant Nose-Throat (Saint) model: a valuable tool to study aerosol deposition in infants. *J. Aerosol Med.* 14(4):433–441, 2001.

[37]Kelly, J. T., B. Asgharian, J. S. Kimbell, and B. Wong. Particle deposition in human nasal airway replicas manufactured by different methods. Part I: inertial regime particles. *Aerosol Sci. Technol.* 38:1063–1071, 2004.

[38]Kelly, J. T., B. Asgharian, J. S. Kimbell, and B. Wong. Particle deposition in human nasal airway replicas manufactured by different methods. Part II: ultrafine particles. *Aerosol Sci. Technol.* 38:1072–1079, 2004.

[39]Kesavanathan, J., R. Bascom, and D. L. Swift. The effect of nasal passage characteristics on particle deposition. *J. Aerosol Med.* 11(1):27–39, 1998.

[40]Kimbell, J. S., J. H. Overton, R. P. Subramaniam, P. M. Schlosser, K. T. Morgan, R. B. Conolly, and F. J. Miller. Dosimetry modeling of inhaled formaldehyde: binning nasal flux predictions for quantitative risk assessment. *Toxicol. Sci.* 64(1):111–121, 2001.

[41]Kundoor, V., and R. N. Dalby. Effect of formulation- and administration-related variables on deposition pattern of nasal spray pumps evaluated using a nasal cast. *Pharm. Res.* 28(8):1895–1904, 2011.

[42]Liu, Y., E. A. Matida, J. Gu, and M. R. Johnson. Numerical simulation of aerosol deposition in a 3-D human nasal cavity using RANS, RANS/EIM, and LES. *J. Aerosol Sci.* 38:683–700, 2007.

[43]Longest, P. W., and J. Xi. Effectiveness of direct Lagrangian tracking models for simulating nanoparticle deposition in the upper airways. *Aerosol Sci. Technol.* 41(4):380–397, 2007.

[44]Longest, P. W., and J. X. Xi. Condensational growth may contribute to the enhanced deposition of cigarette smoke particles in the upper respiratory tract. *Aerosol Sci. Technol.* 42(8):579–602, 2008.

[45]Martonen, T. B., and Z. Zhang. Deposition of sulfate acid aerosols in the developing human lung. *Inhalation Toxicol.* 5(1):165–187, 1993.

[46]Martonen, T. B., Z. Q. Zhang, G. Yue, and C. J. Musante. Fine particle deposition within human nasal airways. *Inhalation Toxicol.* 15(4):283–303, 2003.

[47]Matida, E. A., W. H. Finlay, and L. B. Grgic. Improved numerical simulation of aerosol deposition in an idealized mouth-throat. *J. Aerosol Sci.* 35:1–19, 2004.

[48]Moghadas, H., O. Abouali, A. Faramarzi, and G. Ahmadi. Numerical investigation of septal deviation effect on deposition of nano/microparticles in human nasal passage. *Respir. Physiol. Neurobiol.* 177(1):9–18, 2011.

[49]Moller, W., G. K. Saba, K. Haussinger, S. Becker, M. Keller, and U. Schuschnig. Nasally inhaled pulsating aerosols: lung, sinus and nose deposition. *Rhinology* 49(3):286–291, 2011.

[50]Morgan, K. T., and T. M. Monticello. Airflow, gas deposition, and lesion distribution in the nasal passages. *Environ. Health Perspect.* 85:209–218, 1990.

[51]Mortola, J. P. Breathing pattern in newborns. *J. Appl. Physiol.* 56(6):1533–1540, 1984.

[52]Nasr, H., G. Ahmadi, and J. B. McLaughlin. A DNS study of effects of particle–particle collisions and two-way coupling on particle deposition and phasic fluctuations. *J. Fluid Mech.* 640:507–536, 2009.

[53]Okuyama, K., Y. Kousaka, and K. Hayashi. Change in size distribution of ultrafine aerosol particles undergoing Brownian coagulation. *J. Colloid Interface Sci.* 101(1):98–109, 1984.

[54]Oldham, M. J., R. C. Mannix, and R. F. Phalen. Deposition of monodisperse particles in hollow models representing adult and child-size tracheobroncial airways. *Health Phys.* 72(6):827–833, 1997.

[55]Persak, S. C., S. Sin, J. M. McDonough, R. Arens, and D. M. Wootton. Noninvasive estimation of pharyngeal airway resistance and compliance in children based on volume-gated dynamic MRI and computational fluid dynamics. *J. Appl. Physiol.* 111(6):1819–1827, 2011.

[56]Phalen, R. F., R. G. Cuddihy, R. G. Fisher, O. R. Moss, R. B. Schlesinger, D. L. Swift, and H. C. Yeh. Main features of the proposed NCRP respiratory tract dosimetry model. *Radiat. Prot. Dosimetry* 38:179–184, 1991.

[57]Phalen, R. F., M. J. Oldham, C. B. Beaucage, T. T. Crocker, and J. D. Mortensen. Postnatal enlargement of human tracheobronchial airways and implications for particle deposition. *Anat. Rec.* 212:368–380, 1985.

[58]Pickering, D. N., and C. S. Beardsmore. Nasal flow limitation in children. *Pediatr. Pulmonol.* 27(1):32–36, 1999.

[59]Rasmussen, T. R., A. Andersen, and O. F. Pedersen. Particle deposition in the nose related to nasal cavity geometry. *Rhinology* 38(3):102–107, 2000.

[60]Rusconi, F., M. Castagneto, N. Porta, L. Gagliardi, G. Leo, A. Pellegatta, S. Razon, and M. Braga. Reference values for respiratory rate in the first 3 years of life. *Pediatrics* 94(3):350–355, 1994.

[61]Scherer, P. W., K. Keyhani, and M. M. Mozell. Nasal dosimetry modeling for humans. *Inhalation Toxicol.* 6:85–97, 1994.

[62]Schroeter, J. D., G. J. M. Garcia, and J. S. Kimbell. Effects of surface smoothness on inertial particle deposition in human nasal models. *J. Aerosol Sci.* 42(1):52–63, 2011.

[63]Schroeter, J. D., C. J. Musante, D. M. Hwang, R. Burton, R. Guilmette, and T. B. Martonen. Hygroscopic growth and deposition of inhaled secondary cigarette smoke in human nasal pathways. *Aerosol Sci. Technol.* 34(1):137–143, 2001.

[64]Shi, H., C. Kleinstreuer, and Z. Zhang. Laminar airflow and nanoparticle or vapor deposition in a human nasal cavity model. *J. Biomech. Eng.* 128:697–706, 2006.

[65]Shi, H., C. Kleinstreuer, and Z. Zhang. Modeling of inertial particle transport and deposition in human nasal cavities with wall roughness. *J. Aerosol Sci.* 38:398–419, 2007.

[66]Storey-Bishoff, J., M. Noga, and W. H. Finlay. Deposition of micrometer-sized aerosol particles in infant nasal airway replicas. *J. Aerosol Sci.* 39(12):1055–1065, 2008.

[67]Subramaniam, R. P., R. B. Richardson, K. T. Morgan, J. S. Kimbell, and R. A. Guilmette. Computational fluid dynamics simulations of inspiratory airflow in the human nose and nasopharynx. *Inhalation Toxicol.* 10(2):91–120, 1998.

[68]Swift, D. L., N. Montassier, P. K. Hopke, K. Karpenhayes, Y. S. Cheng, Y. F. Su, H. C. Yeh, and J. C. Strong. Inspiratory deposition of ultrafine particles in human nasal replicate cast. *J. Aerosol Sci.* 23(1):65–72, 1992.

[69]Swift, D. L., and J. C. Strong. Nasal deposition of ultrafine 218Po aerosols in human subjects. *J. Aerosol Sci.* 27(7):1125–1132, 1996.

[70]Tian, L., G. Ahmadi, Z. C. Wang, and P. K. Hopke. Transport and deposition of ellipsoidal fibers in low Reynolds number flows. *J. Aerosol Sci.* 45:1–18, 2012.

[71]Wang, S. M., K. Inthavong, J. Wen, J. Y. Tu, and C. L. Xue. Comparison of micron- and nanoparticle deposition patterns in a realistic human nasal cavity. *Respir. Physiol. Neurobiol.* 166(3):142–151, 2009.

[72]Wheatley, J. R., T. C. Amis, and L. A. Engel. Nasal and oral airway pressure-flow relationships. *J. Appl. Physiol.* 71(6):2317–2324, 1991.

[73]Xi, J., and P. W. Longest. Transport and deposition of micro-aerosols in realistic and simplified models of the oral airway. *Ann. Biomed. Eng.* 35(4):560–581, 2007.

[74]Xi, J., and P. W. Longest. Numerical predictions of submicrometer aerosol deposition in the nasal cavity using a novel drift flux approach. *Int. J. Heat Mass Transf.* 51(23–24):5562–5577, 2008.

[75]Xi, J., and P. W. Longest. Characterization of submicrometer aerosol deposition in extrathoracic airways during nasal exhalation. *Aerosol Sci. Technol.* 43(8):808–827, 2009.

[76]Xi, J., P. W. Longest, and T. B. Martonen. Effects of the laryngeal jet on nano- and microparticle transport and deposition in an approximate model of the upper tracheobronchial airways. *J. Appl. Physiol.* 104(6):1761–1777, 2008.

[77]Xi, J., X. Si, J. W. Kim, and A. Berlinski. Simulation of airflow and aerosol deposition in the nasal cavity of a 5-year-old child. *J. Aerosol Sci.* 42(3):156–173, 2011.

[78]Yamada, Y., Y. S. Cheng, H. C. Yeh, and D. L. Swift. Inspiratory and expiratory deposition of ultrafine particles in a human nasal cast. *Inhalation Toxicol.* 1:1–11, 1988.

[79]Yu, G., Z. Zhang, and R. Lessmann. Fluid flow and particle diffusion in the human upper respiratory system. *Aerosol Sci. Technol.* 28:146, 1998.

[80]Zamankhan, P., G. Ahmadi, Z. Wang, P. K. Hopke, Y. S. Cheng, W. C. Su, and D. Leonard. Airflow and deposition of nano-particles in a human nasal cavity. *Aerosol Sci. Technol.* 40:463–476, 2006.

[81]Zhang, Z., and C. Kleinstreuer. Computational analysis of airflow and nanoparticle deposition in a combined nasal-oral-tracheobronchial airway model. *J. Aerosol Sci.* 42(3):174–194, 2011.

[82]Zhao, K., P. W. Scherer, S. A. Hajiloo, and P. Dalton. Effects of anatomy on human nasal air flow and odorant transport patterns: implications for olfaction. *Chem. Senses* 29(5):365–379, 2004.